Acta Cryst. (1995). B**51**, 768–779

The Low-Temperature Phase Transition Sequence of the Halide Perovskite Tetramethylammonium Trichlorogermanate(II) and the Structure of its Incommensurately Modulated δ-Phase

BY KLAUS FÜTTERER† AND WULF DEPMEIER

Mineralogisches Institut, Universität Kiel, Olshausenstrasse 40, *D*-24098 *Kiel, Germany*

AND VACLAV PETŘÍČEK

Institute of Physics, Academy of Sciences of the Czech Republic, Na Slovance 2, 180 40 *Praha* 8, *Czech Republic*

(*Received* 6 *July* 1994; *accepted* 16 *November* 1994)

Abstract

Tetramethylammonium trichlorogermanate(II), $N(CH_3)_4GeCl_3$, abbreviated as TGC, has been investigated by temperature-dependent X-ray powder and single-crystal diffraction. It is shown that TGC has a one-dimensional incommensurately modulated phase, called the δ-phase, with primary modulation wavevector $\mathbf{q} \approx 0.14\,\mathbf{b}^*$. This phase is stable in the temperature range $170 \leq T \leq 200$ K and occurs between the room-temperature phase γ and a lower-temperature phase ε. The structure of δ-TGC was refined in the (3+1)-dimensional superspace group $Pnam(0\beta0)00s$. The average structure of δ-TGC with lattice parameters $13.083(6) \times 8.841(4) \times 9.027(4)$ Å^3 ($T = 190$ K) is isomorphous to the structure of the normal room-temperature phase γ. The latter is of distorted perovskite-type [Depmeier, Möller & Klaska (1980). *Acta Cryst.* B**36**, 803–807]. The modulation in the case of the δ-phase is purely displacive, the dominant modulation wave being polarized along the *c*-axis and of magnitude 0.42 Å. The low-temperature phase ε is monoclinic with lattice parameters $13.068(6) \times 8.808(5) \times 8.962(6)$ Å^3, $\alpha = 93.9(1)°$ at $T = 160$ K. The intensity of the incommensurate satellite reflections vanishes at the δ–ε transition. The observed diffraction patterns suggest that the δ–ε transition at 170 K is also associated with the partial reappearance of the orthorhombic lattice of the γ-phase. In fact, both single-crystal and powder diffraction display the superposition of a monoclinic and an orthorhombic reciprocal lattice, which persists from $T_{\delta-\varepsilon} = 170$ K down to at least 130 K. The intensity ratio of monoclinic to orthorhombic reflections is *ca* 5:1 and is essentially constant for $T < 160$ K.

Introduction

Halide perovskite-type compounds of general composition ABX_3, with $A = Rb^+$, Cs^+, $N(CH_3)_4^+$,... and B being a subvalent group IV metal ion, *i.e.* Ge^{2+}, Sn^{2+} or Pb^{2+}, show a variety of phases and phase transitions, which have been mainly characterized as order–disorder driven (*e.g.* Fujii, Hoshino, Yamada & Shirane, 1974; Ng & Zuckerman, 1985; Thiele, Rotter & Schmidt, 1987). They have also attracted attention for interesting physical properties, such as their high ionic conductivity in the cubic high-temperature phase (Depmeier, Möller & Klaska, 1980; Mizusaki, Arai & Fueki, 1983; Yamada, Isobe, Okuda & Furukawa, 1994) or, in some cases, the significant change of colour associated with the different phases (Thiele, Rotter & Schmidt, 1989).

In recent years the halide germanates of this series have been extensively studied by X-ray diffraction and Raman scattering (Thiele, Rotter & Schmidt, 1987, 1988, 1989). One of the objectives was to understand the impact of the lone pair on the coordination sphere of Ge^{2+}. As the ability to hybridize increases from Pb to Ge, one expects an increasing stereochemical activity for the lone pair. Accordingly, one finds an increasing tendency in the same direction to form discrete trigonal-pyramidal BX_3^- anions rather than regular BX_6 octahedra.

Up to now, five phases have been reported in the temperature range $130 \leq T \leq 450$ K for TGC. They have been revealed by differential scanning calorimetry [DSC (Möller, 1980)], four of which being confirmed by a recent ^{35}Cl NQR investigation (Yamada, Isobe, Okuda & Furukawa, 1994). Fig. 1 shows this phase transition sequence as a function of temperature.

$T_{\alpha-\beta} = 428$ K	α-Phase	$Pm\bar{3}m$	6.55 Å
$T_{\beta-\gamma} = 390$ K	β-Phase	?	?
$T_{\gamma-\delta} = 200$ K	γ-Phase	$Pnam$	13.07 x 8.89 x 9.12 Å^3
$T_{\delta-\varepsilon} = 170$ K	δ-Phase	$Pnam(0\beta0)00s$	13.08 x 8.84 x 9.03 Å^3
	ε-Phase	monoclinic orthorhombic	13.03 x 8.79 x 8.91 Å^3, α = 94.7° 13.03 x 8.79 x 8.96 Å^3

Fig. 1. Phase diagram of $N(CH_3)_4GeCl_3$ as a function of temperature. $T_{\gamma-\delta}$ and $T_{\delta-\varepsilon}$ are quoted according to the X-ray powder results, $T_{\alpha-\beta}$ and $T_{\beta-\gamma}$ according to the DSC results of Möller (1980).

† To whom correspondence should be addressed. Present address: Research School of Chemistry, Australian National University, Canberra ACT 0200, Australia.

The crystal structure of γ-TGC, *i.e.* the room-temperature structure, was first reported by Depmeier, Möller & Klaska (1980). This refinement was carried out in the non-centrosymmetric space group $Pna2_1$. It showed that the structure is of perovskite-type, but strongly distorted. Yamada, Isobe, Okuda & Furukawa (1994) recently reported a Rietveld refinement of the structure of γ-TGC, which was successfully carried out in the centrosymmetric space group *Pnam* (the space group is given here in the setting corresponding to $Pna2_1$). This discrepancy will be discussed later on. However, from both refinements the formation of discrete trigonal-pyramidal $GeCl_3^-$ groups is obvious and results in a $GeCl_6$ coordination octahedron, which shows rather large non-bonded (Ge···Cl) distances of up to 4.33 Å compared with Ge—Cl bonds of *ca* 2.3 Å length. Thus, it is more appropriate to label the coordination (3+3) rather than sixfold.

The Rietveld refinement of the structure of the cubic α-phase, carried out by Yamada, Isobe, Okuda & Furukawa (1994), suggests that the proper perovskite structure does not occur even in the cubic phase. While it is perovskite-like in terms of the location of the Ge atoms and the TMA molecules, the cubic symmetry actually results from a dynamic disorder of the $GeCl_3$ groups. The model proposed by these authors, in accordance with the earlier proposed model of Depmeier, Möller & Klaska (1980), assumes a rotation of the $GeCl_3$ groups about the triad axis combined with diffusion of the chlorine ions, which accounts for the extraordinarily high ionic conductivity in the α-phase reported by both groups. The Rietveld refinement strongly supports this picture.

While the phase diagram of the halide germanates has been widely studied at and above room temperature, comparatively little attention has been paid to the low-temperature behaviour. The fact that no structural data were available for the two low-temperature phases present in TGC gave the motivation to carry out a temperature-dependent X-ray diffraction study on the title compound. During the course of this investigation it was shown that the δ-phase, which is stable between 170 and 200 K, has an incommensurately modulated structure (Fütterer & Depmeier, 1993). In the present article we report the structural analysis and refinement of this phase, as well as preliminary results on the low-temperature phase ε.

Experimental

Synthesis

Crystals suitable for X-ray structure investigation were grown by a convection method following a procedure given by Möller (1980), from an equimolar solution of $N(CH_3)_4Cl$ and $GeCl_2$ in 5 M HCl. Guinier and precession photographs identified the sample and confirmed its purity.

Temperature-dependent X-ray diffraction

Temperature-dependent powder diffractograms were recorded on a Guinier X-ray diffractometer in steps of 10 K between 300 and 130 K and on a finer scale, *i.e.* $\Delta T = 2$ K, for $160 < T < 220$ K.† For this measurement a Huber G645 diffractometer was used with an attached helium closed-cycle cooling stage (CTI Cryogenics 22C).

Buerger precession photographs of reciprocal lattice layers $h, k, (0, 1, 2)$ and $(0, 1, 2), k, l$ (indices refer to the γ-TGC reciprocal lattice) were recorded at room temperature, 183 and 158 K, using a nitrogen-flow cooling stage (Leybold–Heraeus, TCD 1) and Zr-filtered Mo radiation.

Determination of the modulation wavevector

The modulus of the modulation wavevector $\mathbf{q} = \delta\mathbf{b}^*$ was determined from the peak–peak distance of satellite reflections *hklm* and *hklm̄*, obtained by performing *Q*-scans along $\mathbf{b}^*$. The *Q*-scans were carried out by dividing the interval scanned in reciprocal space into 200 steps, *i.e.* the highest resolution the diffractometer control software could provide. This allowed δ to be determined up to ± 0.001. The temperature dependence of δ was measured in the interval $170 \leq T \leq 200$ in variable steps of 2.5 down to 1 K, determining the peak–peak distance of reflections $006m$ and $006\bar{m}$, $m = 1, 2, 3$. It was carefully checked beforehand, whether δ was the same for different *hkl* and especially for different $l\mathbf{c}^*$.

Data collection

The single crystal data were recorded on a Stoe–Siemens four-circle diffractometer equipped with a cold nitrogen-flow cooling device (Oxford cryostreamer). As we were confined to the use of Mo $K\alpha$ radiation, the short modulation vector, which corresponds approximately to a sevenfold superstructure with $b \approx 63$ Å, could cause overlap of neighbouring main and satellite reflections. To exclude or at least to minimize this problem, the opening aperture of the detector slit was set to its minimum value and the ω-scan technique was chosen for data collection. As the $00l$ reflections revealed a strong temperature dependence within the δ-phase, 004 was chosen as one of the standards, thus providing an indicator for temperature stability. See Table 1 for a summary of the data collection parameters.

The structure refinement

Determination of the superspace group

From the temperature-dependent Guinier powder diffractograms it became obvious that the crystal system

† The numbered intensity of each measured point on the profile has been deposited with the IUCr (Reference JS0007). Copies may be obtained through The Managing Editor, International Union of Crystallography, 5 Abbey Square, Chester CH1 2HU, England.

Table 1. *Parameters of data collection*

Diffractometer	Stoe–Siemens
Radiation	Mo $K\alpha$, graphite monochromator
Scan mode	ω-scan, 25 steps × 0.05°
	0.5–2.0 s per step
Data collection limits in 2θ (°), *hklm*	
$m = 0, 1$	$5 \le 2\theta \le 45$
	$-14 \le h \le 14, -9 \le k \le 9, -10 \le l \le 10$
$m = 2$	$5 \le 2\theta \le 35$
	$-11 \le h \le 11, -7 \le k \le 7, -8 \le l \le 8$
No. of measured reflections	21216, 3177 unique, 1226 with $I \ge 3\sigma(I)$
Standards	800, 060, 004 every 60 min
Orientation check	Every 4 h
Temperature (K)	190
Lattice parameters	
a (Å)	13.083 (6)
b (Å)	8.841 (4)
c (Å)	9.027 (4)
	(determined from 18 reflections with $17 \le 2\theta \le 27.8°$ at 190 K)
Modulation wavevector	$\mathbf{q} = \delta\,\mathbf{b}^*$, $\delta = 0.143$ (1) at 190 K
Lorentz and polarization correction	*REDU*4 software (Stoe & Cie, 1988)
Absorption correction	None

remains orthorhombic across the γ–δ transition. Furthermore, precession photographs recorded of the δ-phase showed systematic extinction conditions for the main reflections compatible with either the centrosymmetric space group *Pnam* or with non-centrosymmetric $Pna2_1$. Proceeding from the earlier successful refinement of γ-TGC in space group $Pna2_1$ (Depmeier, Möller & Klaska, 1980), it was assumed that this space-group symmetry correctly described the average structure of δ-TGC. The (3 + 1)-dimensional superspace group was then derived from the tables of de Wolff, Janssen & Janner (1981) to be $Pna2_1(0\beta0)$ (superspace group notation according to Janssen, Janner, Looijenga-Vos & de Wolff, 1992), in accordance with the systematic extinction conditions observed by the precession photographs.

The subsequent refinement of δ-TGC in $Pna2_1(0\beta0)$ gave reasonable R-values, but quite unsatisfactory bond distances. In addition, it was noticed that atomic positions only slightly deviated from centrosymmetric positions. Therefore, the centrosymmetric superspace groups $Pnam(0\beta0)$ and $Pnam(0\beta0)00s$, which are minimal super groups of $Pna2_1(0\beta0)$, were taken into consideration. While the first implies the same systematic absences as $Pna2_1(0\beta0)$, the second requires in addition $hk0m$, $m = 2n$. There were 11 weak first-order harmonic satellites, which violated this condition showing an intensity greater than $3\sigma(I)$. However, these reflections display an improper peak shape and their intensity could be attributed to tails of neighbouring strong main reflections, as a result of the above-mentioned resolution problem. Thus, from the observed systematic extinction conditions, neither of the two superspace groups could be excluded and therefore further criteria for the choice of the superspace group had to be taken into account.

From the diffraction pattern shown by the precession exposures of reciprocal lattice layers $0kl$ (see Fig. 3) and $hk0$, it could be deduced (Korekawa, 1967) that a purely displacive transverse modulation, polarized along **c**, is present. This is in accordance with the result of the former refinement in the non-centrosymmetric superspace group $Pna2_1(0\beta0)$. This consideration favours the superspace group $Pnam(0\beta0)00s$, since $Pnam(0\beta0)$ does not allow transversal modulation along the c-axis for atoms situated on the (..m)-mirror such as Ge, Cl2 *etc.* Hence, we further assumed $Pnam(0\beta0)00s$ to be the superspace group, which appropriately describes the incommensurate structure of δ-TGC.

Refining the average structure

The average as well as the modulated structure of δ-TGC were refined using the software package *JANA*93 (Petříček, 1993). Table 3 gives the details of the refinement and relevant information. Compared with the description of TGC in $Pna2_1$, the number of atoms in the asymmetric unit reduces from 9 to 7 in the centrosymmetric space group *Pnam*. In *Pnam* the Ge, Cl2, N, C1 and C2 atoms are situated on the mirror plane perpendicular to the c axis, *i.e.* position 4c $(x, y, 3/4)$. This implies that the cross terms U_{13} and U_{23} of the anisotropic thermal parameters U_{ij} of those atoms are zero by symmetry.

Refining the modulated structure

As the displacements of the atoms away from their positions in the underlying average structure are periodic, the atomic modulation function describing these displacements can be expanded in a Fourier series. Usually, the series is expanded up to the order of the measured satellite reflections, which is justified for small modulation amplitudes. In the case of δ-TGC, Fourier terms up to second-order were taken into account. The general atomic modulation function can be expressed accordingly by

$$\begin{aligned}\mathbf{u}(\mathbf{n},\mathbf{r},t) = \mathbf{a}\{&u_{x1}\sin[2\pi(\mathbf{q}(\mathbf{n}+\mathbf{r})+t)]\\ &+ v_{x1}\cos[2\pi(\mathbf{q}(\mathbf{n}+\mathbf{r})+t)]\\ &+ u_{x2}\sin[4\pi(\mathbf{q}(\mathbf{n}+\mathbf{r})+t)]\\ &+ v_{x2}\cos[4\pi(\mathbf{q}(\mathbf{n}+\mathbf{r})+t)]\}\\ &+ \mathbf{b}\{u_{y1}\sin[2\pi(\mathbf{q}(\mathbf{n}+\mathbf{r})+t)]\\ &+ v_{y1}\cos[2\pi(\mathbf{q}(\mathbf{n}+\mathbf{r})+t)]\\ &+ u_{y2}\sin[4\pi(\mathbf{q}(\mathbf{n}+\mathbf{r})+t)]\\ &+ v_{y2}\cos[4\pi(\mathbf{q}(\mathbf{n}+\mathbf{r})+t)]\}\\ &+ \mathbf{c}\{u_{z1}\sin[2\pi(\mathbf{q}(\mathbf{n}+\mathbf{r})+t)]\\ &+ v_{z1}\cos[2\pi(\mathbf{q}(\mathbf{n}+\mathbf{r})+t)]\\ &+ u_{z2}\sin[4\pi(\mathbf{q}(\mathbf{n}+\mathbf{r})+t)]\\ &+ v_{z2}\cos[4\pi(\mathbf{q}(\mathbf{n}+\mathbf{r})+t)]\}, \qquad (1)\end{aligned}$$

where **q** is the modulation wavevector, **n** a Bravais lattice vector, **r** the atomic position in the basic structure and t

the internal coordinate accounting for the fourth dimension in so-called internal space (de Wolff, Janssen & Janner, 1981).

The special position of Ge, Cl2 *etc.* on the m_z-mirror in conjunction with the superspace-group symmetry operation $(m/s)_z$ implies symmetry-determined constraints on the Fourier terms of these atoms. Thus, the atomic modulation function for these atoms is given by

$$\begin{aligned}\mathbf{u}(\mathbf{n},\mathbf{r},t) = \mathbf{a}\{&u_{x2}\sin[4\pi(\mathbf{q}(\mathbf{n}+\mathbf{r})+t)]\\ &+ v_{x2}\cos[4\pi(\mathbf{q}(\mathbf{n}+\mathbf{r})+t)]\}\\ &+ \mathbf{b}\{u_{y2}\sin[4\pi(\mathbf{q}(\mathbf{n}+\mathbf{r})+t)]\\ &+ v_{y2}\cos[4\pi(\mathbf{q}(\mathbf{n}+\mathbf{r})+t)]\}\\ &+ \mathbf{c}\{u_{z1}\sin[2\pi(\mathbf{q}(\mathbf{n}+\mathbf{r})+t)]\\ &+ v_{z1}\cos[2\pi(\mathbf{q}(\mathbf{n}+\mathbf{r})+t)]\}.\end{aligned}$$

The anisotropic thermal parameters U_{ij} were assumed not to be modulated. A total of 103 positional and thermal parameters were refined using 944 reflections with $F \geq 3\sigma(F)$. The final overall residual value was $R = \{\Sigma(F_o - F_c)^2/\Sigma F_o^2\}^{1/2} = 0.0387$.

Results

Results of the temperature-dependent X-ray diffraction

The phase transitions at 200 and 170 K, which have been observed before by DSC (Möller, 1980) and temperature-dependent ^{35}Cl NQR (Yamada, Isobe, Okuda & Furukawa, 1994), are confirmed by the low-temperature X-ray powder results. Fig. 2 shows the temperature evolution of reflections 211, 002 and 020 in the range $160 \leq T \leq 220$ K in steps of 2 K on cooling. Below 200 K weak extra reflections occur in the diffractogram, which can be indexed on the basis of an orthorhombic $13 \times 8 \times 9$ Å^3 lattice and a modulation vector $\mathbf{q} = \delta\mathbf{b}^*$, with $\delta \approx 0.14$. At 170 K a substantial change occurs, resulting in a rather complex diffraction pattern.

Figs. 3 and 4 show Buerger precession photographs of reciprocal layer 0*kl* at 183 and 158 K, respectively, *i.e.* in the δ- and ε-phase. Fig. 3 displays a diffraction pattern consisting of strong main and weaker satellite reflections, pointing to the incommensurate character of the δ-phase. While on first glance the exposure might suggest an

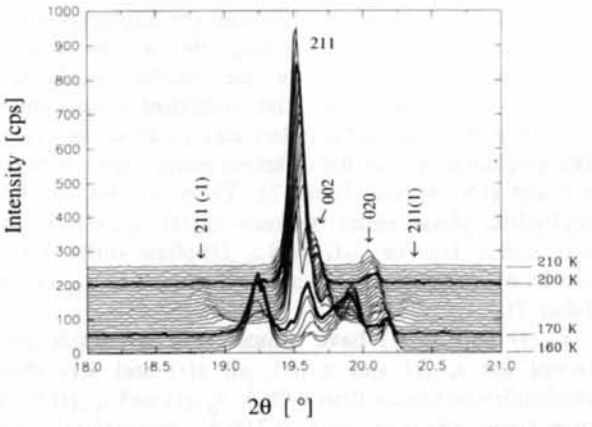

Fig. 2. Thermodiffractogram of reflections 211, 002 and 020 in the temperature range $160 \leq T \leq 220$ K in steps of 2 K at cooling. The diffraction patterns at 170 and 200 K are highlighted. Satellite reflections are indicated with the fourth index in parentheses.

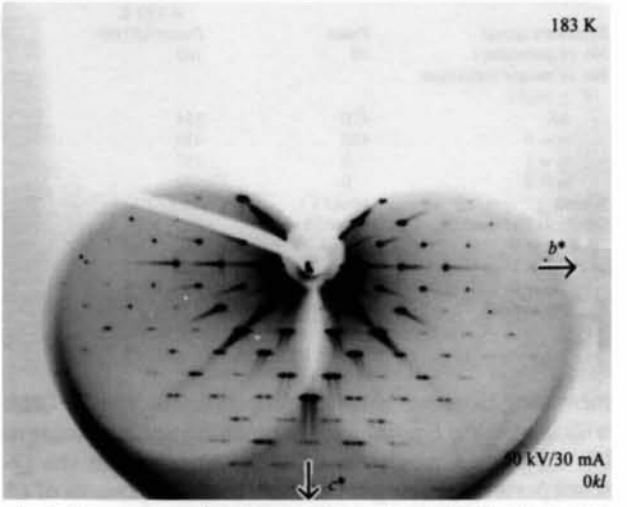

Fig. 3. Buerger precession photograph of reciprocal lattice layer 0*kl* in the δ-phase at 183 K.

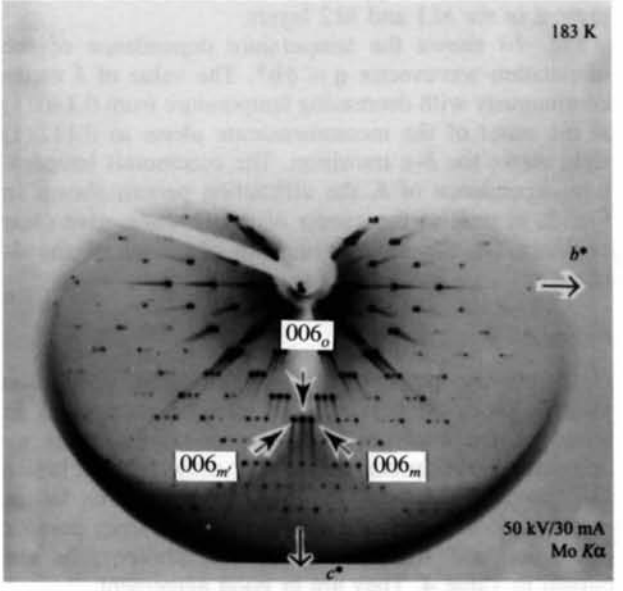

Fig. 4. Buerger precession photograph of reciprocal lattice layer 0*kl* in the ε-phase at 158 K. The subscript *o* refers to the orthorhombic lattice, whereas *m* and *m'* refer to the two monoclinic lattices, which are related by twinning owing to the ferroelastic character of the δ–ε phase transformation.

Table 2. *Value of δ for different components of* **c*** *at* 185 K, *δ defined by* $\mathbf{q} = \delta\,\mathbf{b}^*$

Reflection 00*lm*	$m = 1$	$m = 2$	$m = 3$
002*m*	0.142 (1)	not observed	not observed
004*m*	0.142 (1)	0.142 (8)	not observed
006*m*	0.142 (1)	0.142 (1)	0.142 (3)
00 10*m*	0.143 (2)	0.142 (1)	0.140 (3)

Table 3. *Refinements and relevant parameters*

Refinement run	Average structure	Modulated structure
Modulation wavevector		$\mathbf{q} = \delta\,\mathbf{b}^*$, $\delta = 0.143$ (1) at 190 K
Symmetry group	*Pnam*	*Pnam*(0β0)00*s*
No. of parameters	49	103
No. of unique reflections $F \geq 3\sigma(F)$		
All	410	944
$m = 0$	410	410
$m = 1$	0	457
$m = 2$	0	77
Weight	$1/[\sigma(F)^2]$	$1/[\sigma(F)^2]$
Residuals (%) over all	4.8, 6.35	3.87, 5.20
R, *wR* $m = 0$	4.85, 6.35	4.03, 5.36
$m = 1$	-	3.39, 4.80
$m = 2$	-	5.69, 6.62
R_{exp} (%) over all	6.13	6.13

increasing distance between reflections 0*klm* and 0*klm̄* with increasing *l*, pointing to a twinning perpendicular to **b***, no such dependence could be observed in the *Q*-scans performed along **b*** for different components of **c*** (see Table 2). In fact, a careful analysis of the exposure with a precise evaluation chart was in accordance with the result of the *Q*-scans. It was further noticed that no satellite reflections appeared in the *hk*0 layer, but were present in the *hk*1 and *hk*2 layers.

Fig. 10 shows the temperature dependence of the modulation wavevector $\mathbf{q} = \delta\,\mathbf{b}^*$. The value of δ varies continuously with decreasing temperature from 0.140 (1) at the onset of the incommensurate phase to 0.112 (1) right above the δ–ε transition. The continuous temperature dependence of δ, the diffraction pattern shown in Fig. 3, as well as the results of the *Q*-scans, give clear evidence for the incommensurate character of the δ-phase.

Below the δ–ε transition

The X-ray powder and single-crystal diffraction patterns observed below 170 K can be interpreted in terms of the superposition of a monoclinic and an orthorhombic reciprocal lattice. The orthorhombic lattice is apparently the same as in the γ-phase. The lattice parameters of both lattices as determined from powder diffraction and from the precession photographs are quoted in Table 4. They are in good agreement.

At the δ–ε transition the intensity of the satellite reflections vanishes with $\mathbf{q} \approx 1/9\,\mathbf{b}^*$ right above the phase transformation. The δ–ε transition is associated with a shearing of the orthorhombic unit cell in the *bc*-plane of *ca* 4°. In addition, the orthorhombic lattice of the γ-phase seems to recover at the δ–ε transition. Down to 130 K, the lower limit of our X-ray powder investigation, no complete transformation to the monoclinic phase could be detected. The superposition of the two lattices was obtained at every cooling run, as well as with different samples, although with varying intensity ratios between monoclinic and orthorhombic reflections. The intensity ratio between monoclinic and orthorhombic reflections below 160 K, as estimated from the powder diffraction results, is roughly 5 to 1 and remains essentially constant from $T = 160$ K down to 130 K. All transitions are completely reversible with a hysteresis of *ca* 7 K at the δ–ε transformation.

Table 4. *Lattice parameters of the monoclinic and the orthorhombic lattice in the ε-phase, as determined from the precession photographs and from Guinier powder diffraction*

	Guinier (Å) $T = 160$ K	Precession (Å) $T = 158$ K
Orthorhombic	13.064 (6)	13.03 (1)
	8.788 (5)	8.79 (1)
	8.99 (1)	8.96 (1)
Monoclinic	13.068 (6)	13.03 (1)
	8.808 (5)	8.79 (1)
	8.962 (6)	8.91 (1)
	$\alpha = 93.9$ (1)°	$\alpha = 94.7$ (1)°

Result of the structure refinement

The coordinates and the Fourier coefficients, as well as the thermal parameters, which result from the refinements, are contained in Tables 5 and 6, respectively.

As in the room-temperature phase, the average structure consists of trigonal-pyramidal $GeCl_3^-$ groups forming strongly distorted $GeCl_6$ coordination octahedra. The average structure will be considered in more detail in the *Discussion*.

The atomic modulation functions, as defined by (1), for the atoms of the asymmetric unit are displayed in Fig. 5. Let $x_X(t), y_X(t), z_X(t)$ denote the **a**-, **b**- and **c**-component, respectively, of the atomic modulation function of the atom *X*. The dominant displacement wave is transversal and is polarized parallel to the *c*-axis. The amplitude $z(t)$ for the different atoms varies between 0.3 and 0.57 Å (see Table 7). There are no, or only negligible, phase shifts between $z_{Ge}(t)$, $z_{Cl1}(t)$, $z_{Cl2}(t)$, $z_N(t)$ and $z_{C1}(t)$. For $z_{C2}(t)$ and $z_{C3}(t)$ phase shifts of 39.6 and 21.6°, respectively, occur with respect to $z_{Ge}(t)$ (see Table 7).

$x_{Ge}(t)$ and $y_{Ge}(t)$ have almost zero amplitude and, except for $x_{C2}(t)$ and $x_{C3}(t)$, all $x(t)$ and $y(t)$ show amplitudes no higher than 0.08 Å. $x_{C2}(t)$ and $x_{C3}(t)$ show amplitudes of 0.11 and 0.316 Å, respectively, but obviously give only a minor contribution to the overall diffraction pattern. Thus, $z(t)$ can be regarded as the only relevant displacement wave.

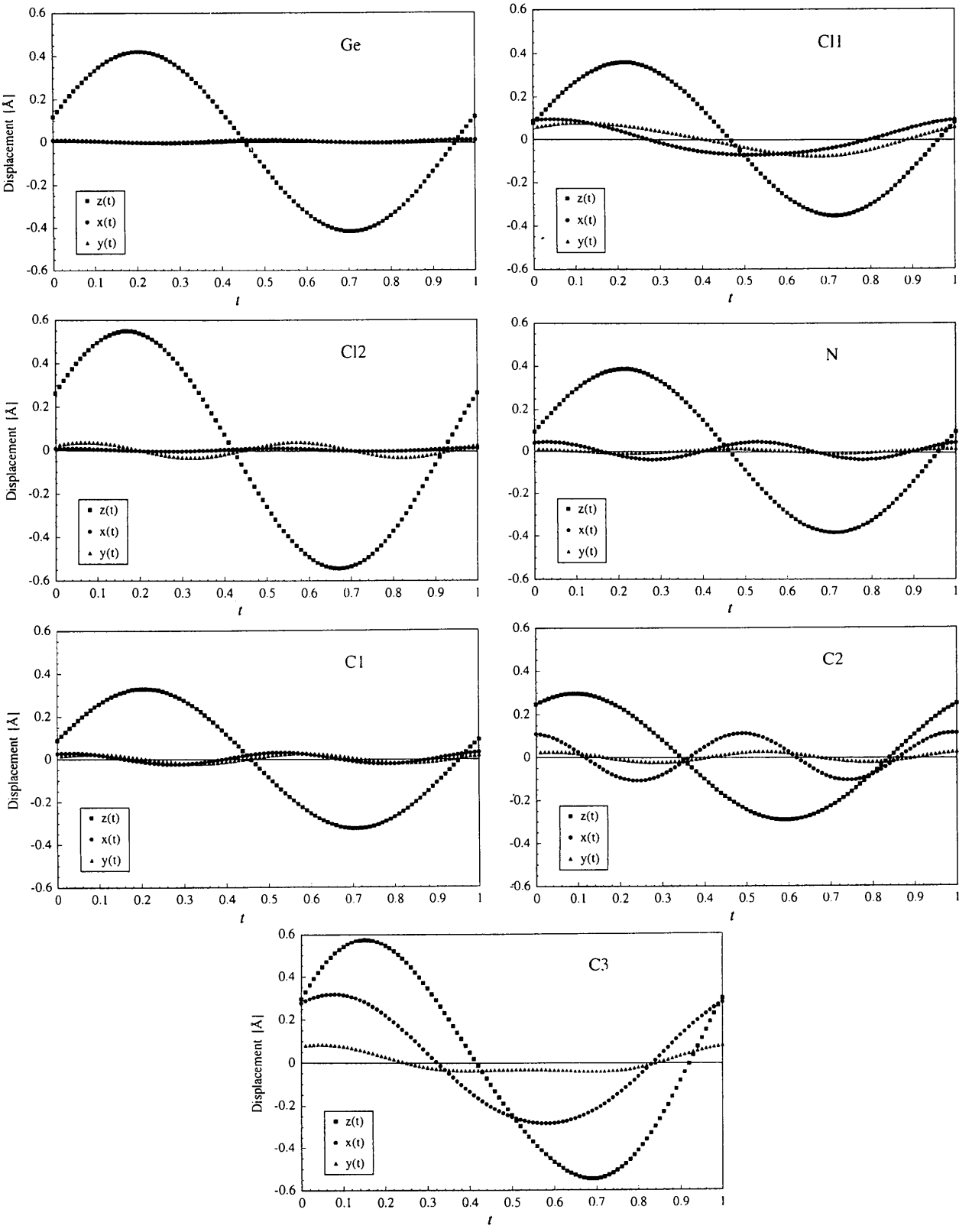

Fig. 5. Periodic displacements of the atoms contained in the asymmetric unit of the average structure as a function of the internal coordinate t in δ-TGC.

Table 5. *Fourier coefficients of atomic modulation functions and coordinates of the average structure, respectively*

		Average structure	Modulated structure				
		r	r	u_1	v_1	u_2	v_2
Ge	x	0.2571 (1)	0.2572 (1)	*	*	0.0002 (2)	−0.0004 (1)
	y	0.2517 (1)	0.2517 (1)	*	*	0.0005 (1)	0.0006 (2)
	z	3/4	3/4	0.0464 (1)	0.0030 (1)	*	*
Cl1	x	0.2701 (1)	0.2701 (1)	−0.0019 (1)	−0.0062 (1)	−0.0006 (2)	−0.0006 (2)
	y	0.0767 (2)	0.0769 (1)	−0.0070 (1)	−0.0051 (1)	0.0001 (3)	0.0009 (3)
	z	0.9384 (2)	0.9382 (2)	0.0392 (2)	0.0059 (1)	0.0001 (2)	0.0001 (2)
Cl2	x	0.4280 (2)	0.4279 (1)	*	*	0.0004 (4)	−0.0004 (4)
	y	0.3153 (3)	0.3152 (2)	*	*	−0.0040 (4)	−0.0004 (3)
	z	3/4	3/4	0.0589 (3)	0.0134 (3)	*	*
N	x	0.4981 (4)	0.4975 (2)	*	*	−0.002 (1)	0.0022 (9)
	y	0.2306 (7)	0.2309 (4)	*	*	0.000 (1)	0.001 (1)
	z	1/4	1/4	0.0427 (6)	−0.0015 (7)	*	*
C1	x	0.4677 (7)	0.4676 (4)	*	*	0.001 (1)	−0.002 (1)
	y	0.0687 (9)	0.0686 (5)	*	*	−0.002 (2)	−0.001 (1)
	z	1/4	1/4	0.0355 (9)	−0.0075 (9)	*	*
C2	x	0.4035 (7)	0.4038 (4)	*	*	−0.004 (1)	0.008 (1)
	y	0.330 (1)	0.3300 (5)	*	*	0.002 (2)	0.002 (2)
	z	1/4	1/4	0.025 (1)	−0.021 (1)	*	*
C3	x	0.5579 (9)	0.5574 (4)	0.0153 (6)	0.0172 (7)	0.001 (1)	0.0003 (9)
	y	0.2622 (9)	0.2630 (5)	0.0031 (8)	0.0058 (7)	0.002 (1)	−0.002 (1)
	z	0.115 (2)	0.1150 (6)	0.0592 (8)	0.0169 (9)	0.004 (1)	−0.0008 (9)

* Coefficients which are by symmetry constrained to zero.

Table 6. *Anisotropic thermal parameters*

The anisotropic temperature factor has the form: $\exp[-2\pi^2(U_{11}h^2a^{*2} + U_{22}k^2b^{*2} + U_{33}l^2c^{*2} + 2U_{12}hka^*b^* + 2U_{13}hla^*c^* + 2U_{23}klb^*c^*)]$.

		U_{11}	U_{22}	U_{33}	U_{12}	U_{13}	U_{23}
Ge	a	0.0548 (7)	0.0479 (7)	0.181 (1)	0.0120 (5)	†	†
	m	0.0555 (3)	0.0465 (3)	0.0705 (5)	0.0119 (2)	†	†
Cl1	a	0.066 (1)	0.072 (1)	0.128 (2)	0.0023 (9)	−0.007 (1)	−0.015 (1)
	m	0.0613 (6)	0.0663 (6)	0.0535 (6)	−0.0008 (5)	0.0021 (5)	−0.0001 (5)
Cl2	a	0.072 (2)	0.047 (1)	0.296 (5)	−0.015 (1)	†	†
	m	0.074 (1)	0.0454 (8)	0.104 (1)	−0.0146 (7)	†	†
N	a	0.037 (4)	0.032 (4)	0.17 (1)	0.000 (3)	†	†
	m	0.039 (2)	0.033 (2)	0.059 (3)	−0.001 (2)	†	†
C1	a	0.069 (6)	0.030 (5)	0.15 (1)	−0.002 (4)	†	†
	m	0.067 (3)	0.031 (3)	0.090 (5)	−0.004 (3)	†	†
C2	a	0.057 (6)	0.046 (5)	0.18 (1)	0.016 (4)	†	†
	m	0.049 (4)	0.046 (3)	0.126 (6)	0.013 (3)	†	†
C3	a	0.167 (8)	0.071 (6)	0.27 (1)	0.008 (5)	0.15 (1)	0.031 (7)
	m	0.111 (4)	0.074 (3)	0.094 (4)	0.000 (3)	0.060 (4)	0.016 (3)

a = average structure, m = modulated structure.
† Coefficients which are by symmetry constrained to zero.

Table 7. *Maximum displacement of atoms from average positions*

Atom	x_{max} (Å)	y_{max} (Å)	z_{max} (Å)	Phase shift* [°]
Ge	0.007	0.007	0.419	0
Cl1	0.074	0.08	0.358	0
Cl2	0.007	0.036	0.546	14.4
N	0.042	0.011	0.386	0
C1	0.026	0.023	0.327	0
C2	0.11	0.024	0.295	39.6
C3	0.316	0.044	0.548	21.6

* Phase shift of $z_X(t)$ with respect to $z_{Ge}(t)$.

The variation of bond distances and angles (see Table 8) implied by the modulation is only small. Bonds in the $GeCl_3$ group vary by 0.008 Å, compared with an e.s.d. of 0.002 Å for the average value. The respective angles at the Ge vary by less than 1.8° (e.s.d. $\simeq$ 0.05°). The same applies basically for the bonds within the $N(CH_3)_4^+$ cation, where the respective quantities vary by *ca* 0.1 Å (e.s.d. $\simeq$ 0.007 Å) and 5° (e.s.d. $\simeq$ 0.2°). As the modulation amplitude of the individual atoms is of the order 0.4 Å, both the $GeCl_3$ group and the TMA cation can be looked upon as rigid bodies to a very good approximation.

Discussion

The average structure of δ-TGC

The refinement of the average structure of δ-TGC shows that it is isomorphous to the crystal structure of γ-TGC (Yamada, Isobe, Okuda & Furukawa, 1994;

Table 8. *Bond distances* (Å) *and angles* (°), *selected non-bonded distances and related angles*

Refinement run	Average structure	Modulated structure mean value	Δ
Ge—Cl1	2.305 (2)	2.305 (1)	[0.008]
Ge—Cl2	2.305 (3)	2.306 (2)	[0.007]
Cl1—Ge—Cl1	95.08 (8)	95.13 (4)	[0.25]
Cl1—Ge—Cl2	95.30 (3)	95.33 (2)	[1.71]
N—C1	1.49 (1)	1.487 (6)	[0.063]
N—C2	1.52 (1)	1.514 (7)	[0.116]
N—C3	1.48 (1)	1.503 (7)	[0.065]
C1—N—C2	109.8 (4)	109.8 (2)	[1.7]
C1—N—C3	108.9 (3)	108.9 (2)	[3.8]
C2—N—C3	108.9 (3)	108.9 (2)	[5.9]
Non-bonded distances			
Ge···Cl1′	4.037 (2)	4.040 (1)	[0.276]
Ge···Cl2′	4.347 (3)	4.348 (2)	[0.022]
Ge···Ge′	6.320 (1)	6.3211 (6)	[0.261]
Ge···Ge″	6.542 (1)	6.5417 (8)	[0.009]
N···N′	6.083 (6)	6.087 (3)	[0.191]
N···N″	6.562 (6)	6.560 (4)	[0.281]
N···N‴	6.551 (8)	6.550 (5)	[0.110]
C···Cl distances			
C1···Cl1	3.820 (7)	3.823 (6)	[0.094]
C1···Cl2	3.660 (9)	3.663 (5)	[0.029]
C2···Cl1	3.581 (8)	3.591 (5)	[0.233]
C2···Cl2	3.83 (1)	3.843 (6)	[0.161]
C3···Cl1	3.78 (1)	3.515 (6)	[0.240]
C3···Cl2	3.74 (1)	3.738 (6)	[0.279]
Angles within the Ge-coordination octahedron			
Cl1—Ge···Cl1	176.58 (6)	176.03 (3)	[5.81]
Cl1—Ge···Cl2	88.95 (5)	88.95 (3)	[4.85]
Cl2—Ge···Cl1	84.95 (6)	84.97 (3)	[4.75]
Cl2—Ge···Cl2	173.69 (8)	173.06 (5)	[2.56]
Cl1···Ge···Cl1	88.34 (4)	88.31 (3)	[0.45]
Cl1···Ge···Cl2	90.54 (4)	90.56 (2)	[2.38]
Angles at Cl atoms			
Ge—Cl1···Ge	170.13 (7)	169.94 (4)	[7.08]
Ge—Cl2···Ge	158.0 (1)	157.56 (6)	[1.87]

Δ = max − min.

Depmeier, Möller & Klaska, 1980). The inherent low accuracy of the powder results in the former of these refinements and the possibly incorrect choice of space group in the latter refinement means that the results have to be compared cautiously with the present results. [A reinvestigation of the structure of γ-TGC by single-crystal X-ray diffraction is underway (Depmeier & Klaska, 1994).] With this limitation in mind, one can nonetheless state that no significant change of the geometries of the $GeCl_3$ anion and the TMA cation occurs across the γ–δ transition. The Ge—Cl bond lengths are in accordance with published values ($\langle d_{Ge-Cl}\rangle = 2.320 \pm 0.016$ Å; Christensen & Rasmussen, 1965; Messer, 1978; Möller, 1980; Thiele, Rotter & Schmidt, 1987). The same applies for the C—N bond lengths ($\langle d_{C-N}\rangle = 1.51 \pm 0.02$ Å; Allen, Kennard, Watson, Brammer, Orpen & Taylor, 1992). The geometry of the TMA cation, as emerging from the refinement, is almost perfectly tetrahedral, with bond angles $\angle$(C—N—C) = 109.2 ± 0.5°.

The hybridization state of Ge^{2+} has formally been described as $4p^3$ with the lone pair occupying the 4*s* state (Depmeier, Möller & Klaska, 1980). This would imply that the lone pair is stereochemically inactive. The structural distortions present in the average structure, however, point to a stereochemically active lone pair. For example, a rotation of the $GeCl_3$ groups about an axis parallel to **c** is observed, resulting in an angle of 14.1° between the Ge—Cl2 bond and the *ac*-plane (see Fig. 6 for illustration). This rotation increases the distance between the lone pair and the neighbouring Cl atoms. In addition, the TMA cations are shifted from $(\frac{1}{2},\frac{1}{4},\frac{1}{4})$ parallel to **b** in the direction of the supposed location of the lone-pair orbital by *ca* 0.16 Å. These shifts could be rationalized, assuming that the presence of an attractive interaction between the cation and the lone pair is plausible. An appropriate formal description of the hybridization state of Ge taking into account an stereochemically active lone pair would then be $4sp^3$.

In order to elucidate the role of the lone pairs (abbreviated as Lp) in more detail, we tried to localize the lone pair by applying the geometrical models proposed by Galy, Meunier, Andersson & Åström (1975) and Hyde & Andersson (1989). However, none of the geometries proposed seems to be fully adequate for the case of TGC, as may be shown by the following examples:

(1) For large anion/cation radius ratios, as for example in $PbCl_2$, Hyde & Andersson (1989) suggest choosing a polyhedron formed by the anions at the corners, the lone pair at its centre and the cation located off-centre. For

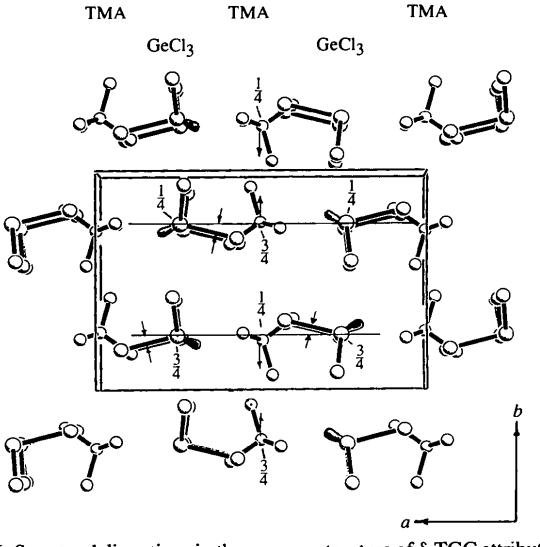

Fig. 6. Structural distortions in the average structure of δ-TGC attributed to the stereochemical activity of the lone pair at the Ge^{2+}. The projection of the structure is down the *c*-axis. The *z*-position of Ge and N atoms are given in fractional coordinates. The shifts of the TMA cations and the rotation of the $GeCl_3$ anions about an axis parallel **c** are indicated by the respective arrows (see *Discussion* for further explanation).

TGC an obvious polyhedron would be an octahedron, constructed with the constraints $d_{Cl2-Lp} = d_{Cl2'-Lp}$ and $d_{Cl1-Lp} = d_{Cl1'-Lp}$. This approach leads to a Ge—Lp distance of 1.65 Å, which seems too long compared with the value of 1.05 Å reported by Hyde & Andersson (1989) on the basis of the structure of GeF_2.

(2) For compounds with smaller anion/cation radius ratios such as *e.g.* ClF_3 or α-PbO, Hyde & Andersson (1989) suggest putting the three anions and the lone pair on the corners of a regular polyhedron, *i.e.* a tetrahedron in the case of TGC. This approach leads to a Ge—Lp distance of 1.58 Å, which still seems much too high.

Thus, barely on the basis of the structure and without the assistance of further criteria, it is hardly possible to determine reliably the location of the lone pair in the present case.

Among other features, the structure of γ-TGC as well as of the average structure of δ-TGC are characterized by a shift of the Ge atoms out of the high symmetry position $(\frac{1}{4}, \frac{1}{4}, \frac{3}{4})$ occupied in the cubic α-phase. The displacement vectors are of modulus 0.1 Å and point approximately in the direction of the orthorhombic *a*-axis. Depmeier, Möller & Klaska (1980) showed that they are arranged in an antiferroelectric-type ordering scheme, as allowed by the centrosymmetric space group *Pnam* (see Fig. 7). An analogous, but in this case ferroelectric-type, ordering of these shifts is found in the room-temperature phase of $CsGeCl_3$ (Christensen & Rasmussen, 1965; Thiele, Rotter & Schmidt, 1987).

The modulated structure of δ-TGC

The modulation with **q** parallel to **b*** and the overall dominant displacement wave component $z(t)$ suggests regarding the structure as consisting of layers of $GeCl_3$ and $N(CH_3)_4$ groups oriented perpendicular to **a**. These layers are located at $x_{GeCl3} \approx \frac{1}{4}, \frac{3}{4}$ and at $x_{TMA} \approx 0$ and $\frac{1}{2}$, respectively. $GeCl_3$ molecules belonging to the same layer are related by symmetry elements, which map **q** onto **q**, and those belonging to adjacent layers (and which are 'nearest neighbours') are related by symmetry elements, which turn **q** into **−q**. By contrast, 'nearest neighbour' TMA cations are mapped onto each other by '**q**→ **−q**' symmetry elements, regardless, whether they belong to the same or to two successive layers.

Within one $GeCl_3$ layer there are two 'translationally independent' Ge atoms (marked with Ge and Ge′ in Fig. 8) related by the $(n/1)_x$-glide plane. The phase shift between two of these atoms is $\Delta\varphi = 2\pi\mathbf{q}\cdot\mathbf{b}/2 \approx 25°$.

Because of the in-phase relationship between $z_{Ge}(t)$ and $z_N(t)$, the distances between Ge and the surrounding N vary only slightly by ±0.06 Å, corresponding to a relative variation of *ca* 2%. The variation of (Ge···Ge) distances of germaniums belonging to adjacent layers is of the same order (see Ge—Ge″ in Table 8), as implied by their symmetry relationship. In conclusion, one can say there is only negligible 'motion' among adjacent $GeCl_3$ layers, but considerable 'motion' within the same layer. This can also be exemplified by the variation of the non-bonded (Ge···Cl) distances within the coordination octahedron $\Delta d_{Ge\cdots Cl2} = 0.022$ and $\Delta d_{Ge\cdots Cl1} = 0.276$ Å, respectively, as well as by the corresponding angle variation of $\Delta\angle$(Ge—Cl2···Ge) = 1.87° and $\Delta\angle$(Ge—Cl1···Ge) = 7.08°, where Δ denotes the difference between the maximum and minimum of the respective quantity. The relation between the TMA cation layers with respect to the distance variation is different from that only in magnitude. Here, the interlayer distance variation is $\Delta d_{N\cdots N'''} = 0.11$ Å compared with the intralayer distance variation, which is $\Delta d_{N\cdots N'} = 0.191$ Å and $\Delta d_{N\cdots N''} = 0.281$ Å.

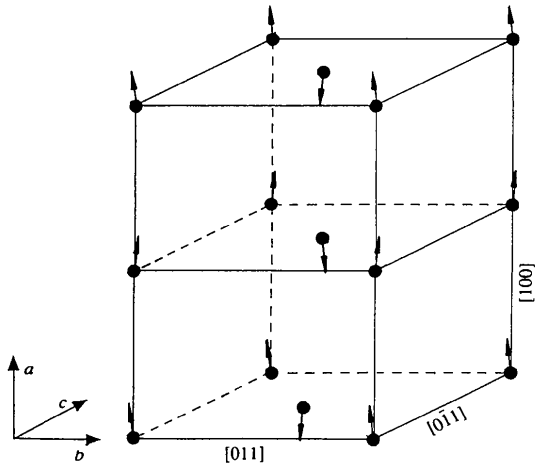

Fig. 7. γ-TGC and average structure of δ-TGC: antiferroelectric ordering of shifts of the Ge atoms with respect to their positions in the cubic α-phase. The modulus of the displacement vectors is *ca* 0.1 Å. Adapted from Depmeier, Möller & Klaska (1980).

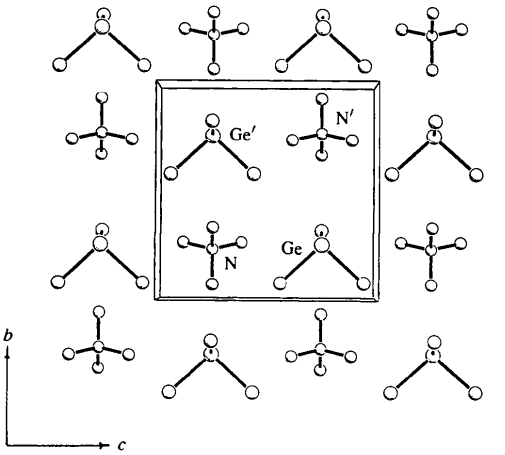

Fig. 8. Projection of the average structure of δ-TGC down the *a*-axis. The $GeCl_3$ layer at $x \approx \frac{1}{4}$ and the TMA layer at $x \approx \frac{1}{2}$ are shown (see *Discussion* for further explanation).

On the possible structural origin of the modulation

Seeking a possible explanation of the modulation, the following experimental observations will be considered: First, the modulation is essentially a pure shear wave running along the **b**-direction with major displacements along **c**. Second, the lattice parameters a, b and c display a uniform linear decrease from room temperature down to $T_{\gamma-\delta} = 200$ K. By contrast, at the γ–δ transition the slope $\partial a/\partial T$ becomes almost zero, whereas $\partial b/\partial T$ and $\partial c/\partial T$ even increase at the phase transformation (see Fig. 9). Finally, γ-TGC shows unusually high thermal parameters U_{33} (Depmeier, Möller & Klaska, 1980), such that the individual atoms suffer a mean square displacement of up to 0.37 Å, as for Cl2. On the basis of these observations, the following model for the formation of the modulated phase is conceivable:

Because of the high U_{33} values it can be assumed that each $GeCl_3$ layer is modulated already in the γ-phase. However, the modulations of adjacent layers will then be uncorrelated, which might be due to static or dynamic disorder. Either way, no satellite reflections can be observed. The distance between adjacent layers decreases with decreasing temperature until they are 'in contact'. This happens at the γ–δ transition, which is marked by the drastic change of the slope $\partial a/\partial T$. As the layers make contact, their motion becomes coherent and the mode corresponding to the modulation condenses out.

Obviously, the present model does not yet account for the occurrence of the modulation within each layer. Here, we are not yet able to make a definite statement.

The low-temperature ε-phase

The transition from the incommensurate δ-phase to the ε-phase is still far from being understood and surely needs further investigation. However, we would like to make the following points.

The shearing of the unit cell in the *bc*-plane by *ca* 4° connected with the transition from the orthorhombic to

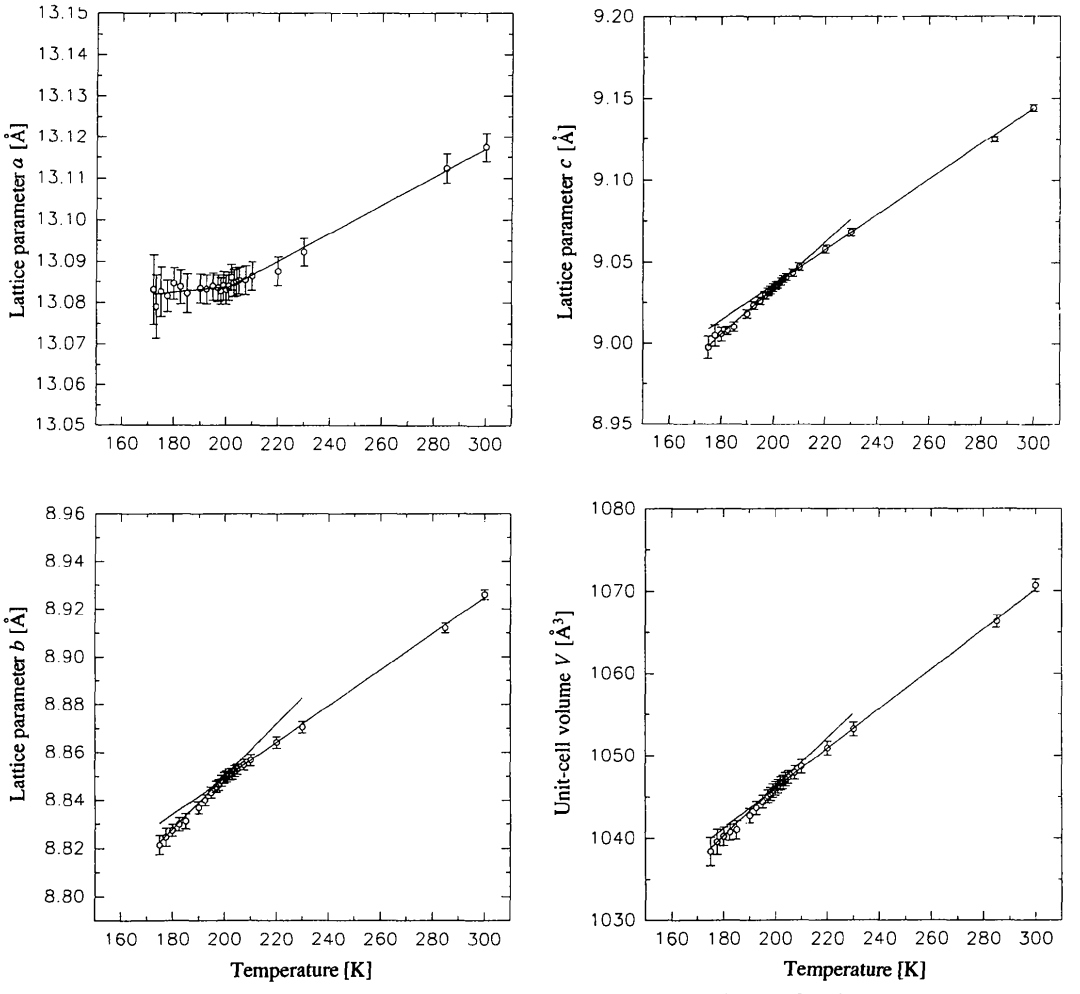

Fig. 9. Orthorhombic lattice parameters and unit-cell volume of $N(CH_3)_4GeCl_3$ as a function of temperature.

the monoclinic lattice is the same shearing of the unit cell imposed locally by the modulation wave in the δ-phase.

The superposition of two different Bravais lattices is observed by single-crystal and powder diffraction, which makes it highly likely that twinning is not the origin of the observed phenomenon.

A few further examples are known to us from the literature, where similar observations have been made, *i.e.* $(Pb_{1-x}Ba_x)_3(PO_4)_2$ (Hensler, Boysen, Bismayer & Vogt, 1993), $1T$-TaS_2 (Withers & Steeds, 1987) and Pb_2CoWO_6 (Sciau, Calvarin, Sun & Schmid, 1992; Rabe & Schmid, 1993). In the Ba-doped lead phosphate, the occurrence of two different lattices coexisting at the same temperature has been attributed to chemical inhomogeneity, although being present on a scale below 1 micron. It is hardly conceivable that such an inhomogeneity has to be taken into consideration in the case of the title compound.

As the two following examples show, chemical inhomogeneity is not necessarily a prerequisite for the coexistence of two different phases. In the charge-density wave system $1T$-TaS_2, the coexistence of two different incommensurate states, the so-called T- and $1T_2$-phases, over a range of 20 K was observed by transmission electron microscopy. Dark-field imaging revealed the formation of domains on a scale of 1 micron (Withers & Steeds, 1987). As pointed out by the authors, their samples were of high chemical purity, because otherwise a certain low-temperature phase, $1T_3$, could not have been observed.

In Pb_2CoWO_6 the coexistence of the intermediate, monoclinic incommensurate phase and the low-temperature, orthorhombic commensurate phase was observed by X-ray diffraction (Sciau, Calvarin, Sun & Schmid, 1992) and by polarized light microscopy (Rabe & Schmid, 1993). The temperature range of coexistence of both phases was observed to be strongly sample-dependent, reaching from $\Delta T = 5$ to $\Delta T \geq 170$ K and being apparently related to the size of domains observed by polarized light microscopy.

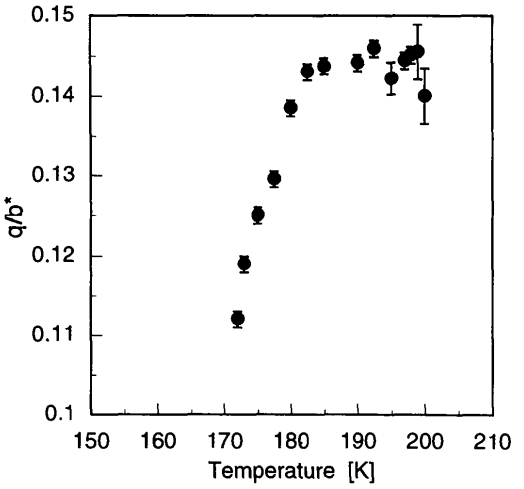

Fig. 10. Modulation wavevector $\mathbf{q} = \delta \mathbf{b}^*$ as a function of temperature.

Concluding remarks

As far as we are aware in the literature, δ-TGC is the first incommensurate phase found in the system of halide perovskites. The origin of the modulation is not yet fully understood. Understanding is also still lacking for the phase sequence $\gamma \rightarrow \delta \rightarrow \varepsilon$. The elucidation of the mechanism of the low-temperature phase transition sequence obviously needs and deserves further experimental efforts.

We would like to thank Professor A. D. Rae and Dr R. L. Withers for valuable discussions, as well as H. H. Eulert and Dr K. F. Hesse for their support in carrying out the low-temperature single-crystal X-ray diffraction experiments. The research work of VP has been made possible by grant 2202/93/1154 from the Grant Agency of the Czech Republic. The Guinier powder diffractometer was made available by the Deutsche Forschungsgemeinschaft under contract No. DE 412-1/2.

References

ALLEN, F. H., KENNARD, O., WATSON, D. G., BRAMMER, L., ORPEN, A. G. & TAYLOR, R. (1992). *International Tables for Crystallography*. Vol. C. pp. 685–706. Dordrecht: Kluwer Academic Publishers.

CHRISTENSEN, A. N. & RASMUSSEN, S. E. (1965). *Acta Chem. Scand.* **19**, 421–428.

DEPMEIER, W. & KLASKA, K.-H. (1994). Personal communication.

DEPMEIER, W., MÖLLER, A. & KLASKA, K.-H. (1980). *Acta Cryst.* B**36**, 803–807.

FUJII, Y., HOSHINO, S., YAMADA, Y. & SHIRANE, G. (1974). *Phys. Rev. B*, **9**, 4549–4559.

FÜTTERER, K. & DEPMEIER, W. (1993). *Acta Cryst.* A**49**, C441.

GALY, J., MEUNIER, G., ANDERSSON, S. & ÅSTRÖM, A. (1975). *J. Solid State Chem.* **13**, 142–159.

HENSLER, J., BOYSEN, H., BISMAYER, U. & VOGT, T. (1993). *Z. Kristallogr.* **206**, 213–231.

HYDE, B. G. & ANDERSSON, S. (1989). *Inorganic Crystal Structures*. New York: Wiley.

JANSSEN, T., JANNER, A., LOOIJENGA-VOS, A. & DE WOLFF, P. M. (1992). *International Tables for Crystallography*, Vol. C, pp. 797–835. Dordrecht: Kluwer Academic Publishers.

KOREKAWA, M. (1967). Habilitationsschrift. Ludwig-Maximilians Universität München, Germany.

MESSER, D. (1978). *Z. Naturforsch. Teil B*, **33**, 366–369.

MIZUSAKI, J., ARAI, K. & FUEKI, K. (1983). *Solid State Ionics*, **11**, 203–211.

MÖLLER, A. (1980). PhD thesis. Univ. Konstanz, Germany.

NG, S. W. & ZUCKERMAN, J. J. (1985). *Adv. Inorg. Chem. Radiochem.* **29**, 297–325.

PETŘÍČEK, V. (1993). *JANA*93. *Programs for Modulated and Composite Crystals*. Institute of Physics, Praha, Czech Republic.

RABE, H. & SCHMID, H. (1993). *Ferroelectrics*, **161**, 49–54.

SCIAU, P., CALVARIN, G., SUN, B. & SCHMID, H. (1992). *Phys. Status Solidi*, **129**, 309–321.

STOE & CIE (1988). *REDU*4. *Data Reduction Program*. Version 6.2. Stoe & Cie, Darmstadt, Germany.

THIELE, G., ROTTER, H. W. & SCHMIDT, K. D. (1987). *Z. Anorg. Allg. Chem.* **545**, 148–156.
THIELE, G., ROTTER, H. W. & SCHMIDT, K. D. (1988). *Z. Anorg. Allg. Chem.* **559**, 7–16.
THIELE, G., ROTTER, H. W. & SCHMIDT, K. D. (1989). *Z. Anorg. Allg. Chem.* **571**, 60–68.
WITHERS, R. L. & STEEDS, J. W. (1987). *J. Phys. C Solid State Phys.* **20**, 4019–4041.
WOLFF, P. M. DE, JANSSEN, T. & JANNER, A. (1981). *Acta Cryst.* A**37**, 625–636.
YAMADA, K., ISOBE, K., OKUDA, T. & FURUKAWA, Y. (1994). *Z. Naturforsch. Teil A*, **49**, 258–266.

Acta Cryst. (1995). B**51**, 779–789

Determination of the Incommensurately Modulated Structure of (Perylene)Co(mnt)$_2$-(CH$_2$Cl$_2$)$_{0.5}$ by Direct Methods

BY ERWIN J. W. LAM, PAUL T. BEURSKENS AND JAN M. M. SMITS

Crystallography Laboratory, Research Institute for Materials, University of Nijmegen, Toernooiveld, 6525 ED Nijmegen, The Netherlands

SANDER VAN SMAALEN* AND JAN L. DE BOER

Laboratory of Chemical Physics, Materials Science Center, University of Groningen, Nijenborgh 4, 9747 AG Groningen, The Netherlands

AND HAI-FU FAN†

Institute of Physics, Chinese Academy of Sciences, PO Box 603, Beijing 100080, People's Republic of China

(*Received* 22 *September* 1994; *accepted* 9 *December* 1994)

Abstract

For the organic conductor (perylene)Co(mnt)$_2$-(CH$_2$Cl$_2$)$_{0.5}$, where mnt is maleonitriledithiolate, the incommensurate displacive modulation is determined using X-ray diffraction data for main reflections and first- and second-order satellites, collected at a temperature of 283 K. The lattice parameters of the unit cell of the average structure are: $a = 6.5441$ (13), $b = 11.7173$ (15), $c = 16.4251$ (17) Å, $\alpha = 92.092$ (11), $\beta = 95.343$ (16), $\gamma = 94.67$ (2)°, with $V = 1248.6$ (3) Å^3 and $Z = 2$. The components of the modulation wavevector are given by: $q_1 = 0.211$ (13), $q_2 = -0.1374$ (5), $q_3 = -0.368$ (2). The symmetry of the modulated structure is given by the (3+1)-dimensional superspace group $P\bar{1}$ (q_1, q_2, q_3). Direct methods were used to obtain a starting model for the modulation. The subsequent refinement converged to $R = 0.126$ for 2835 observed ($I/\sigma > 2.5$) reflections. Partial R factors are 0.111 for 1450 main reflections, 0.143 for 1188 first-order satellites and 0.263 for 197 second-order satellites. The modulation is described by sawtooth-shaped functions for the Co and S atoms and by rigid-body modulations, up to third-order harmonics, for the perylene units and parts of the mnt fragments. The largest amplitudes were found for the Co (0.77 Å) and S atoms (0.48–0.63 Å) and were mainly directed along the a axis. The four equatorial Co—S distances are only slightly affected by the modulation, but the two apical Co—S distances show large variations with distances ranging from 2.05 to 3.86 Å. These variations are out of phase. This causes the coordination of the Co atom to vary from a distorted octahedral coordination by six S atoms to a region with fivefold coordination and *vice versa*. The valence of the Co atom, as calculated by the bond-valence method, varies between 2.92 and 3.57. The stacking of the Co(mnt)$_2$ units can be described by oligomeric packages of four or five dimerized Co(mnt)$_2$ units.

1. Introduction

(Perylene)Co(mnt)$_2$(CH$_2$Cl$_2$)$_{0.5}$ (denoted PECO) belongs to a series of molecular conductors based on perylene (Fig. 1*a*) and metal bis(dithiolenes) of the type M(mnt)$_2$ (Fig. 1*b*) with the general formula (perylene)$_n$M(mnt)$_2$, where M is a metal atom, mnt is maleonitriledithiolate and $n = 1, 2$. The average structure of PECO at room temperature is triclinic, space group $P\bar{1}$ with two formula units in the unit cell (Gama *et al.*, 1992). The structure contains polymeric chains of Co(mnt)$_2$ units, alternated

* Present address: Mineralogisch-Petrographisches Institut und Museum der Universität, Olshausenstrasse 40, D-24098 Kiel, Germany.
† Visiting the Crystallography Laboratory, Research Insitute for Materials, University of Nijmegen, Toernooiveld, 6525 ED Nijmegen, The Netherlands.